

The Structure of Molecular Clouds: III - A link between cloud structure and star formation mode

Jonathan Rowles^{1*} Dirk Froebrich^{1†}

¹*Centre for Astrophysics & Planetary Science, The University of Kent, Canterbury, Kent CT2 7NH, U.K.*

Accepted Received ; in original form

ABSTRACT

We analyse extinction maps of nearby Giant Molecular Clouds to forge a link between driving processes of turbulence and modes of star formation. Our investigation focuses on cloud structure in the column density range above the self shielding threshold of 1 mag A_V and below the star formation threshold – the regime in which turbulence is expected to dominate.

We identify clouds with shallow mass distributions as cluster forming. Clouds that form stars in a less clustered or isolated mode show a steeper mass distribution. Structure functions prove inadequate to distinguish between clouds of different star formation mode. They may, however, suggest that the turbulence in the average cloud is governed by solenoidal forcing. The same is found using the Δ -variance analysis which also indicates that clouds with a clustered mode of star formation show an enhanced component of compressive driving in the turbulent field. Thus, while star formation occurs in each cloud, independent of the turbulent driving mechanism, compressive forcing appears to be associated with the formation of stellar clusters.

Key words: star formation – extinction – ISM: clouds – ISM: dust – ISM: molecules

1 INTRODUCTION

Stars form due to the local collapse of material in molecular clouds. The conditions prior to the collapse result from a complex interplay between self-gravity, turbulence, magnetic fields and thermodynamics. Understanding the effects of each of these influences leads to a better knowledge of how stars form. In this paper we are interested in the role played by interstellar turbulence and its effect on the structure of Giant Molecular Clouds (GMCs).

The subject of astrophysical turbulence is complex and not fully understood, though there are many useful reviews on the topic (e.g. Elmegreen & Scalo (2004), Scalo & Elmegreen (2004), Brandenburg & Nordlund (2009)). Here we are interested in comparing the structure of nearby GMCs to investigate whether it has an influence on the observed star formation properties. Ultimately this might also be used to determine the nature of the turbulent field, i.e. driven by a compressive forcing or solenoidal driving (e.g. Federath et al. (2010)).

We will probe the column density structure in nearby GMCs by means of extinction maps derived from near-infrared observations. This is the least biased way to estimate column density (Goodman et al. (2009)). In the first paper in this series (Rowles & Froebrich (2009), hereafter Paper I), we presented new all-sky extinction maps derived using data from the 2 Micron All-Sky Sur-

vey (2MASS, Skrutskie et al. (2006)). We used the *median* near-infrared colour excess technique (NICE) to calculate the extinction (see Lada et al. (1994)). The nearest 25, 49 and 100 stars to the centre of each pixel were used, hence the noise can be considered constant throughout the map. These extinction maps are therefore referred to as *con-noise* maps.

In our second paper (Froebrich & Rowles (2010), hereafter Paper II), we analysed the column density and mass distributions of a selection of 16 nearby GMCs. To facilitate this we determined new extinction maps using only the stars within each pixel (i.e. no oversampling), which therefore have a constant spatial resolution and are referred to as *con-res* maps. As a result of the analysis we found a universal star formation threshold of about 6.0 ± 1.5 mag A_V . This threshold separates two different regions in the clouds. Below the threshold, at low column densities, turbulence dominates the structure, while at higher column densities gravity is the dominant force. The low A_V part of the clouds could be fitted by a log-normal distribution. There were significant differences in the slopes of the column density and mass distributions when considering only the low A_V regions. This shows that the properties of the turbulence differ depending on the environment of the cloud. Regarding the high A_V regions, we found no such differences, implying that gravity solely dominates these parts.

Using our extinction maps we can derive column density structure functions similar to velocity structure functions (e.g. Padoan et al. (2002)) for each molecular cloud. This will allow us to perform a comparison with models of interstellar turbulence. Pre-

* E-mail: jr262@kent.ac.uk,

† E-mail: df@star.kent.ac.uk

dictions of structure functions resulting from a turbulent medium have been presented e.g. by Schmidt et al. (2008), Kolmogorov (1941), She & Leveque (1994) and Boldyrev (2002) (hereafter S08, K41, SL94 and B02, respectively).

In this paper we test for correlations between structure function parameters and the properties of the clouds. We also examine the cloud structures using the Δ -variance technique (see Stutzki et al. (1998) and Ossenkopf et al. (2008a)) and in particular the mass spectral index scaling coefficient. In Sec. 2 we describe the methods used for our analysis. In Sec. 3 we give the results for the clouds selected. We discuss these results and give conclusions in Secs. 4 and 5, respectively.

2 METHOD

2.1 Structure functions

The general definition of the structure function is given in Eq. 1, (e.g. Lombardi et al. (2008); Padoan et al. (2002) and Padoan et al. (2003)). Here the equation is expressed in terms of our observable – the column density or optical extinction A_V .

$$S_p(\Delta r) = \langle |A_V(r') - A_V(r' - \Delta r)|^p \rangle \quad (1)$$

Δr is the distance between points, r' represents a position in the map, A_V is the optical extinction at r' (or $r' - \Delta r$) and p is the order of the structure function. For $p = 2$ the equation is the two-point correlation function of the extinction map. The brackets $\langle \rangle$ denote that the average over all pixel positions r' and all possible directions for the separation Δr of points is applied. For each order p we find the scaling exponent $s(p)$ by fitting a power-law to values of $S_p(\Delta r)$ against Δr . This assumes that the scaling exponents are related to the structure functions by Eq. 2 (e.g. Padoan et al. (2003)):

$$S_p(\Delta r) \propto \Delta r^{s(p)}. \quad (2)$$

Equation 2 allows us to determine the scaling exponents $s(p)$ which are then normalised to the third order $s(3)$, as a universal behaviour should be exhibited at low Reynolds numbers (determined by Benzi et al. (1993)).

For each GMC investigated we used the range of spatial scales Δr from 0.1 pc to 1.0 pc to fit the power law exponent, in order to be able to compare the results for all clouds. We then follow Padoan et al. (2002) and assume the column density scaling exponents $s(p)/s(3)$ are equivalent to the velocity scaling exponents $\zeta(p)/\zeta(3)$ (Dubrulle (1994)). They can then be expressed by a relation of the form as shown in Eq. 3.

$$\frac{\zeta(p)}{\zeta(3)} = (1 - \Delta)^{\frac{p}{3}} + \frac{\Delta}{1 - \beta}(1 - \beta^{p/3}) \quad (3)$$

Here β is the intermittency and Δ is related to the co-dimension C and intermittency by: $\Delta = C \cdot (1 - \beta)$. The fractal dimension D of the cloud is related to the co-dimension by $D = 3 - C$. Using this equation, the K41 relation can be expressed by setting $\Delta = 0$. As mentioned previously we use the projected column density scaling parameter s instead of the velocity scaling parameter ζ to keep the same description of the structure function as in Padoan et al. (2002), though it is not known *a priori* whether the parameters correspond to each other. However, Padoan et al.

(2002) found that the scaling exponents derived from integrated intensity images follow the velocity scaling using the B02 relation.

We may then derive the parameters Δ , C , β and D for each cloud and compare with the velocity field structure functions obtained from the aforementioned theoretical works by K41, SL94, B02 and S08. When fitting our data to Eq. 3, we varied Δ in the range 0.02 to 1.20 with increments of 0.01, and C ranged from 0.02 to 3.00 with increments of 0.01 to find the best match. Only fits with an *rms* better than 0.1 (in units of $s(p)/s(3)$) were considered a good fit. This is justified given that *rms* is not an absolute measure of the goodness of fit.

Regarding the previously published models, the simplest to consider is that of K41. The energy over a wide range of lengths (known as the ‘inertial range’) in turbulent flows is redistributed from larger scales into ever smaller scales until the effects of viscosity become important. In K41, Kolmogorov considered the structure velocity functions S_2 and S_3 , showing that both are power laws of the form of Eq. 2, with the exponents being $2/3$ and 1 , respectively. Due to the self-similarity of turbulence at different scales, this law can be extended to all powers of p such that $s(p) = p/3$.

However, experimental measurements for the scaling exponents show a deviation from the K41 relation for turbulence, for higher orders of p – known as *intermittency*. This is exhibited in the non-Gaussian tails when plotting the probability density functions (PDFs) of e.g. the column density, and anomalous scaling of higher order structure functions (e.g. Anselmet et al. (1984)). Therefore, we need a relation for the scaling that considers the effects of intermittency.

SL94 derived a scaling relation that accounts for intermittency. Their relation shows good agreement when compared to simulations of structures that are not influenced by magnetic fields. For incompressible turbulence SL94 derived that $C = 2$ and $\Delta = 2/3$. Therefore, the SL94 model assumes that $D = 1$, i.e. that the most intermittent structures are filaments.

B02 extended the SL94 relation to model highly supersonic turbulence and also take account of magnetic fields. They found that $C = 1$ with $\Delta = 2/3$ as with the SL94 model. Under the B02 model it follows that $D = 2$, i.e. that the structures are sheet-like in form.

In S08, the scaling exponents were found to be well described by log-Poisson models. In these models $\Delta \simeq 1$, rather than $2/3$. The modelling applied two types of forcing to drive the turbulence, solenoidal (divergence-free) and compressive (rotation-free). Values for the parameters Δ and C differ depending on the type of forcing applied. Perhaps the nature of forcing in real clouds can be found by comparing the observational data with the S08 model.

2.2 The effect of noise on the structure functions

To ascertain the effect of noise in the data when calculating structure functions from an image we undertook a number of tests. In particular we desired to know whether (increased) random noise leads to a significant and/or systematic deviation of $s(p)/s(3)$ compared to a test image without noise, or a low noise A_V map. In the first instance we made an artificial A_V map of 400×400 pixels containing a circle of radius 124 pixels, where the pixel values in the circle are varied linearly from 0.81 mag (edge) to 10.0 mag (centre). This may be considered analogous to a perfectly spherical cloud with a smooth density variation from the core to the edge (admittedly, an unlikely scenario in practice). All other pixels in the map were set to zero. The structure function of this map happened to correspond to Kolmogorov type turbulence. We then

added 0.28 mag Gaussian noise (corresponding to the 1σ noise in our 49th nearest neighbour map – see Paper I) to this map and fit the parameters Δ , C , β and D . This process was continued by adding further amounts of noise to the basic map with 0.28 mag (1σ) noise. The quantities added were a further 0.0625σ , 0.125σ , 0.1875σ and 0.25σ , generating five images in total. The results of this exercise are discussed in Sec. 3.2.

In addition to investigating the effect of noise on artificial clouds, we added random noise to a selection of real clouds. The clouds chosen were Chameleon, Circinus, Corona Australis, Orion A and Orion B. We used the nearest 49th nearest neighbour A_V maps and added 0.0625σ , 0.125σ , 0.1875σ and 0.25σ noise. We performed the structure function analysis as with the artificial clouds. These results are also discussed in Sec. 3.2.

2.3 The Δ -variance

The Δ -variance method for analysing molecular cloud structures in astronomical images (i.e. in two dimensions) was introduced by Stutzki et al. (1998) and improved by Ossenkopf et al. (2008b). The method works by measuring the quantity of structure on a particular length scale (e.g. Δr) and filtering the data $f(\Delta r)$ with a spherically symmetric ‘down-up-down’ type function. The function (denoted $\odot_l(\Delta r)$), which treats different regimes of Δr separately, is given by Eq. 4 below.

$$\odot_l(\Delta r) = \odot_{l,core}(\Delta r) - \odot_{l,ann}(\Delta r) \quad (4)$$

The RHS of Eq. 4 is defined using Eqs. 5 and 6.

$$\odot_{l,core}(\Delta r) = \frac{4}{\pi l^2} \exp\left(\frac{\Delta r^2}{(l/2)^2}\right) \quad (5)$$

$$\odot_{l,ann}(\Delta r) = \frac{4}{\pi l^2(\nu^2 - 1)} \left[\exp\left(\frac{\Delta r^2}{(\nu l/2)^2}\right) - \exp\left(\frac{\Delta r^2}{(l/2)^2}\right) \right] \quad (6)$$

The Δ -variance, $\sigma_{\Delta}^2(\Delta r)$ is then defined in Eq. 7.

$$\sigma_{\Delta}^2(l) = \left\langle \left(f(\Delta r) * \odot_l(\Delta r) \right)^2 \right\rangle \quad (7)$$

The filter function $\odot_l(\Delta r)$ denotes the Fourier transform of the filter function with size l and diameter ratio ν . Two particular filter types were found to best probe the structure in molecular clouds, a ‘Mexican hat’ filter and a ‘French hat’ filter (Ossenkopf et al. (2008a)). Both filters treat the core and the annulus separately (Eq. 4). The optimal filter function for molecular clouds was found to be either a Mexican hat filter with a diameter ratio of 1.5, (or a French hat filter with a diameter ratio of 2.3 - Ossenkopf et al. (2008a)). We used a Mexican hat filter with a diameter ratio of 1.5 for our analysis.

We applied this method to our *con-noise maps*. To further investigate the dimensions of structures in the clouds (i.e. filaments etc.) we also applied this method to the corresponding star density maps. The structure shown in the star density maps is enhanced since the extinction in the A_V maps is roughly proportional to the log of the star density. Therefore, both the A_V and star density maps were used for this analysis. The results are shown in Sec. 3.3.

Using the Δ -variance technique allows us to also calculate the mass spectral index scaling exponent (denoted α) of each cloud.

This is found by fitting a power-law to σ_{Δ}^2 against scale. The power law is fitted over the range of size of the cloud, i.e. between the smallest and largest scales of the cloud. The smallest scale is determined by eliminating the pixels affected by oversampling. For the largest scale we chose the point where the increase in σ_{Δ}^2 begins to tail off before the peak. These results are also shown in Sec. 3.3.

2.4 The effect of noise on the Δ -variance

As with the structure functions it is also necessary to consider the effects of noise on the Δ -variance results. This was investigated in a similar way as for the structure functions (see Sec. 2.2). The same set of test images of 400×400 pixels containing a circle, as well as real clouds were used. The Δ -variance of these image was calculated. Increments of Gaussian noise were added to each of the images in exactly the same way as for the structure function analysis. The results are presented in Sect. 3.4.

2.5 Molecular cloud density

We estimate the average physical density of the cloud material in order to relate it to the cloud properties obtained from our analysis of the column density and the star formation properties. The average density of material can be estimated from the mass of the cloud M above a certain A_V threshold, the number of pixels N the cloud is covering in our A_V map with values above this threshold, and the distance d to the cloud in the following way:

$$\rho[M_{\odot}/pc^3] = \frac{8.78 \cdot 10^{15} \cdot M[M_{\odot}]}{N^{\frac{3}{2}} \cdot (x''[d[pc]])^3}, \quad (8)$$

Here the average density is expressed in solar masses per cubic parsec, the mass in solar masses, the pixel size x in arcsec and the distance d in parsec. The power of $3/2$ at the number of pixels of the cloud assumes that the two visible dimensions in the plane of the sky are a good representation of the dimension along the line of sight. Note that if one wants to express the density in units of particles per cubic centimeter, then the constant $8.78 \cdot 10^{15}$ needs to be multiplied by a factor of 40.

We determine two average densities for the purpose of this paper. i) The average density of the entire cloud. This includes all material which is above the self shielding column density threshold of 1 mag A_V . ii) The average density of the material above the cloud’s star formation threshold. This corresponds to the density of the material which is potentially involved in star formation. The results are shown in Sect. 3.5.

3 RESULTS

3.1 Structure function results

For the analysis of the structure functions we used the three available *con-noise maps* (see Paper I) for the following reasons:

i) The noise has a less predictable effect on the results when using the *con-res* maps. This is caused by the fact that each pixel has a different number of stars contributing to the A_V value, and hence variable noise. In some cases only very few stars are used. One drawback of using the *con-noise maps* for this analysis is the variable spatial resolution between pixels. This is most notable in

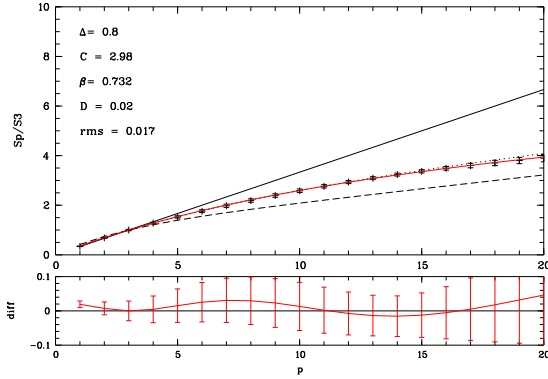


Figure 1. A plot showing the variation of $s(p)/s(3)$ against p for the Auriga 1 cloud and the 49th nearest neighbour map. Our data (+ signs) is compared against the models of K41 (solid line), SL94 (dotted line) and B02 (dashed line). The best fit values of Δ , C , β , D and the rms value are shown in the upper left corner. A plot of the difference of the fit from the data against p is shown as a red solid line in the lower panel.

regions of high extinction. However, we only include pixel separations above 0.1 pc (see above), which are generally above the spatial resolution. Furthermore, we determine the structure functions only for the parts of the cloud where turbulence dominates, i.e. where A_V is greater than 1 mag and less than the cloud's individual star formation threshold (generally below 8 mag, see Paper II).

ii) The obtained values for $s(2)$ and $s(3)$ are very low when using the *con-res* maps. This could be a result of the generally higher and, more importantly, variable noise in these maps. With the *con-noise* maps we found much more reasonable values for $s(2)$ and $s(3)$. We calculate a mean value for $s(2)$ of 0.8 ± 0.4 and $s(3)$ of 1.1 ± 0.6 . For individual clouds, using Taurus as an example, we find $s(2)=0.98$ and $s(3)=1.41$, compared to $s(2)=0.77$ and $s(3)=1.10$ (Padoan et al. (2003)). For Perseus we find $s(2)=1.24$ and $s(3)=1.75$, compared to $s(2)=0.83$ and $s(3)=1.18$.

Thus, we determine the structure function of every GMC for each of the three available A_V maps, utilising only extinction values above the self-shielding limit (1 mag) and below the star formation threshold of the particular cloud. Note that every individual extinction value used for these calculations has a signal-to-noise ratio of at least three (Paper I). Hence, the obtained structure functions are highly reliable, as indicated by the small uncertainties for $s(p)/s(3)$ (e.g. Fig. 1).

For each of the three structure functions we determine the best fitting set of parameters Δ , C , β and D , and a scatter for each parameter by considering only the fits with an rms of less than 0.1 (in units of $s(p)/s(3)$). The final structure function parameters for each cloud are then determined as weighted averages of the three obtained values. An example plot showing $s(p)/s(3)$ against p for the Auriga 1 cloud together with the best fit is shown in Fig. 1, where we used the 49th nearest neighbour map. Similar plots for all clouds are shown in the Appendix A1.

The determined parameters of the structure function (Δ , C , β and D) for all the clouds and their uncertainties are listed in Table 1. The rms of the fit is also shown. The values for Δ lie in the range 0.45 to 1.08 with a mean of 0.85 ± 0.16 . Therefore, even after allowing for uncertainties, the values are more or less in the middle

of those quoted in the literature ($\Delta=2/3$ in e.g. Padoan et al. (2003), SL94, B02; $\Delta=1$ in e.g. Schmidt et al. (2008)).

The co-dimension values C lie between 1.18 and 2.51 with a mean of 1.92 ± 0.37 . In turn the fractal dimension of our sample of clouds has a value of 1.08 ± 0.37 , rendering them filament like rather than sheet like.

The values of β (the degree of non-intermittency) in our sample range from 0.38 to 0.65 with a mean of 0.53 ± 0.08 . The literature usually quotes a values for β of either $2/3$ (SL94) or $1/3$ (B02). Therefore, the value for our GMC sample lies about halfway between these values.

3.2 The effect of noise on the structure functions

We added noise to a test image and to a selection of the extinction maps of real clouds to investigate the effect on the structure functions and their fitted parameters (Δ , C , β , D ; see Sec. 2.2). The results of this exercise are shown in Table 2.

In the top part of the table we list the values of the structure function parameters obtained for our test image and the test image plus noise. As one can see, the artificial cloud corresponds to a structure in agreement with Kolmogorov type turbulence ($\Delta \approx 0$). This also implies that the actual values of the other parameters are meaningless (see Eq. 3). Once our typical noise of 0.28 mag A_V has been added the parameters change significantly. The values for Δ are 0.5 and the structure corresponds to an almost two-dimensional object ($D=1.9$). When the noise is further increased no systematic and/or significant changes are observed. This has two implications: i) Our typical noise can change the structure function parameters significantly compared to a column density map which is free of noise. ii) Once the image has some observational noise, a small increase in the noise will not change the values of the determined structure function parameters significantly or systematically. All changes are well below the uncertainties of the parameters. This implies that it does not matter which of our A_V maps we use (and indeed justifies that we average the results from all three maps), as the variation of a factor of two in the number of stars leads only to an increase/decrease of the noise in the maps by 33 % (caused in part by the covariance, see Paper I).

The bottom part of Table 2 illustrates the latter part of the above discussion for a real cloud (Corona Australis). With the standard noise in the 49th nearest neighbour map of 0.28 mag A_V we obtain the listed values for the structure function parameters. When increasing the noise by another small amount (at maximum 25 %), again we do not find any significant and/or systematic changes in the determined structure function parameters.

3.3 Δ -variance results

We applied the Δ -variance technique (as described in Sec. 2.3) to all GMCs of our sample. As an example we show the results of the σ_Δ^2 plot for Orion A in Fig. 2. Similar plots for all the individual clouds can be found in the Appendix A1. These plots also contain a cut-out of the 49th nearest neighbour A_V map, as well as the structure function of the cloud, determined from this map.

The statistical error bars for the Δ -variance in some clouds appear rather large. This has also been recognised by Ossenkopf et al. (2008a). However, they also note that (quote): "In spite of the large error bars, the general scaling behaviour can be accurately traced." Since we will measure the mass spectral index scaling exponents α in these diagrams we determined the weighted correlation coefficients r_α (listed in the last column of Table 1). They show, except

Table 1. Summary of the results for the 16 investigated GMCs. The table lists the cloud name (see Paper II for coordinate ranges); the best fitting structure function parameters from Eq. 3 and their uncertainties (see text for details); values of the slopes $s(2)$ and $s(3)$; average cloud density of material with an A_V above 1 mag; average cloud density of material above the star formation threshold (note that $1 \text{ M}_\odot/\text{pc}^3$ corresponds to 40 cm^{-3}); scale of the peak in the Δ -variance analysis; scale of the peak in the Δ -variance analysis when applied to the star density maps (a — denotes that no peak is visible); the mass spectral index scaling exponent and its uncertainty from the Δ -variance analysis; weighted correlation coefficient for the determination of the mass scaling exponent; †Low density probably caused by large distance (800 pc) of cloud and hence partially unresolved higher density material. ‡High density due to the fact that the cloud is situated in a region with a general background/foreground extinction. Clouds labeled with ¹ are part of the group with steep column density and mass distributions, and clouds labeled with ² are part of the group with shallow distributions according to Paper II.

Name	Δ	σ_Δ	C	σ_C	β	σ_β	D	σ_D	rms	σ_{rms}	$s(2)$	$s(3)$	ρ_{av} [M_\odot/pc^3]	ρ_{SF}	$\widehat{\sigma}_{\Delta^2}^{A_V}$ [pc]	$\widehat{\sigma}_{\Delta^2}^\rho$ [pc]	α	σ_α	r_α
² Auriga 1	0.77	0.07	2.05	0.55	0.59	0.13	0.95	0.55	0.05	0.01	1.15	1.66	4.9	99	—	10	0.36	0.07	0.980
² Auriga 2	0.45	0.20	1.18	0.63	0.57	0.14	1.82	0.63	0.04	0.01	0.70	0.99	12	1900	—	—	0.49	0.13	0.944
² Cepheus	0.85	0.21	2.31	0.40	0.62	0.12	0.69	0.40	0.05	0.02	0.86	1.27	5.2	190	16.0	—	0.18	0.10	0.984
¹ Chamaeleon	0.96	0.06	2.51	0.34	0.62	0.04	0.49	0.34	0.05	0.02	0.72	1.05	29	520	3.5	—	0.63	0.09	0.949
¹ Circinus	1.01	0.07	1.67	0.38	0.38	0.10	1.33	0.38	0.06	0.02	0.33	0.44	4.0	42	—	—	0.69	0.03	0.997
¹ Corona Australis	0.88	0.07	2.28	0.45	0.60	0.08	0.72	0.45	0.04	0.02	0.66	0.93	58	1500	—	1.0	1.08	0.03	0.989
² λ -Ori	0.90	0.11	2.05	0.47	0.54	0.13	0.95	0.47	0.05	0.02	0.65	0.92	6.9	100	12.0	4.0	0.17	0.03	0.425
² Lupus 1 and 2	1.02	0.08	1.92	0.47	0.45	0.12	1.08	0.47	0.06	0.02	0.34	0.47	8.3	680	1.5	—	0.23	0.10	0.644
² Lupus 3, 4, 5, 6	1.08	0.07	2.23	0.51	0.49	0.14	0.77	0.51	0.06	0.02	-0.01	0.02	8.3	1500	3.8	—	0.41	0.04	0.963
² Monoceros	0.93	0.06	1.97	0.45	0.51	0.09	1.03	0.45	0.05	0.01	1.06	1.43	1.3†	23	6.0	—	0.18	0.04	0.923
¹ Ophiuchus	0.74	0.11	1.69	0.54	0.54	0.11	1.31	0.54	0.05	0.02	1.31	1.89	18	3400	1.5	1.25	0.71	0.06	0.975
¹ Orion A	0.66	0.28	1.22	0.55	0.42	0.21	1.78	0.55	0.05	0.02	1.14	1.58	12	310	11.0	2.0	0.95	0.16	0.976
¹ Orion B	0.83	0.09	2.05	0.58	0.57	0.11	0.95	0.58	0.05	0.02	1.33	1.91	7.0	580	—	—	0.52	0.05	0.950
¹ Perseus	0.79	0.12	1.75	0.51	0.53	0.08	1.25	0.51	0.04	0.01	1.24	1.75	15	1600	—	1.8	0.64	0.12	0.992
¹ Serpens	0.95	0.07	1.63	0.38	0.40	0.10	1.37	0.38	0.06	0.02	0.17	0.22	100‡	860	—	1.5	0.73	0.03	0.957
¹ Taurus	0.75	0.25	2.14	0.55	0.65	0.09	0.86	0.55	0.04	0.01	0.98	1.41	32	6500	3.5	0.5	0.61	0.10	0.950

Table 2. Structure function parameters obtained by our test with increased noise. We list the noise added to the image (in units of 0.28 mag A_V , the 1σ noise in our 49th nearest neighbour map) and the structure function parameters as well as the rms . **Top:** Results when adding noise to our artificial test image. **Bottom:** Example for the test with a real cloud, in this case Corona Australis. We only used the 49th nearest neighbour map, and the original image is thus represented by the first line. The noise values for this case hence represent the total noise, not just the added noise.

Noise [σ]	Δ	σ_Δ	C	σ_C	β	σ_β	D	σ_D	rms	σ_{rms}
artificial test cloud										
0.0000	0.02	0.01	2.03	0.58	0.99	0.01	0.97	0.58	0.01	0.01
1.0000	0.50	0.06	1.18	0.41	0.55	0.11	1.82	0.41	0.04	0.01
1.0625	0.50	0.06	1.21	0.42	0.55	0.10	1.79	0.42	0.04	0.01
1.1250	0.48	0.06	1.09	0.40	0.53	0.12	1.91	0.40	0.05	0.01
1.1875	0.48	0.06	1.17	0.43	0.56	0.11	1.83	0.43	0.04	0.01
1.2500	0.44	0.06	0.96	0.38	0.49	0.14	2.04	0.38	0.05	0.01
Corona Australis										
1.0000	0.85	0.03	2.64	0.25	0.68	0.02	0.36	0.25	0.09	0.01
1.0625	0.83	0.06	2.35	0.41	0.64	0.04	0.65	0.41	0.03	0.01
1.1250	0.83	0.06	2.39	0.41	0.65	0.04	0.61	0.41	0.03	0.01
1.1875	0.86	0.06	2.42	0.40	0.64	0.04	0.58	0.40	0.03	0.01
1.2500	0.92	0.05	2.57	0.33	0.64	0.03	0.43	0.33	0.04	0.01

for two clouds (λ -Ori, Lupus 1, 2) that there is a very good correlation, with r_α generally significantly larger than 0.9.

Using our *con-noise* maps we investigated the positions of the peaks in the Δ -variance plots. These peaks reveal the scale at which a change in the structure occurs, e.g. the size of the cloud, the length of filaments etc.. These results are shown in Table 1. We find peaks in some of the clouds (Cepheus, Chamaeleon, λ -Ori, Orion A, Lupus, Monoceros, Taurus) while for the remaining clouds no clear-cut peak can be identified. The identified peaks appear over a range of scales from 1.5 pc (Lupus 1 and 2 and Ophiuchus) to 16 pc (Cepheus).

Using the star density instead of the column density maps, we find peaks in the Δ -variance for the clouds Auriga 1, Circinus, Corona Australis, λ -Ori, Ophiuchus, Orion A, Perseus, Serpens and Taurus. In general, the peaks occur at smaller scales (from 0.5 pc in Taurus to 10 pc in Auriga 1). However, only for four clouds (λ -Ori, Ophiuchus, Orion A, Taurus) do we detect a clear peak in both maps. In each case we find that the peak determined when using the column density map is larger, indicating that the star density maps trace smaller scales when the Δ -variance technique is applied to them.

By means of the *con-noise* maps we also measure the mass spectral index scaling exponents α for each cloud. These values and uncertainties are listed in the last two columns of Table 1. The listed values are the mean of the results for the three available column density maps. The values for α range from 0.17 (λ -Ori) to 1.08 (Corona Australis) with a mean for all clouds of 0.54 ± 0.27 .

3.4 The effect of noise on the Δ -variance

Similar to the investigations of the structure function, we determined the influence of noise on our analysis of the cloud structure with the Δ -variance method. The same noise increments as for the structure function analysis were added to the extinction maps and the change to the peak position of the Δ -variance and the mass spectral index scaling exponent were determined.

Neither the peak position nor the mass spectral index seem to be significantly and/or systematically influenced, if an additional noise of the level discussed in Sect. 2.2 is added to the extinction maps. This applies to both, the use of our artificially generated image as well as the real cloud. Hence the obtained values can be considered robust.

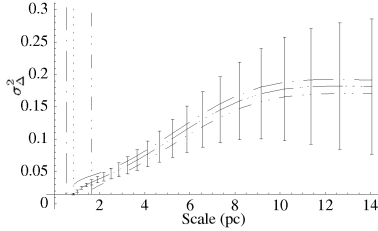


Figure 2. Example of the delta variance σ_{Δ}^2 for Orion A. We show the results for all three available A_V maps (*dash-dot* 25th nearest neighbours, *dotted* 49th nearest neighbour, *dash-dot-dot* 100th nearest neighbours). The corresponding vertical lines indicate the spatial resolution limit for each map, below which the values are meaningless. The typical scale of the structure in this cloud can be identified by the peak at about 11 pc. For clarity, error bars are only overplotted on the 49th nearest neighbour data. The weighted correlation coefficient for the determined slope is 0.976.

3.5 Molecular cloud density

The determined average densities of the entire GMCs, as well as the densities of the material above the star formation threshold can be found in Table 1.

The average densities for the entire cloud range from $1.3 M_{\odot}/pc^3$ (for Monoceros) to $100 M_{\odot}/pc^3$ (for Serpens). The low value for Monoceros might be due to small scale structures not being detected because of the distance to the cloud. For the Serpens cloud the apparently high density is due to a general offset in the extinction values (either foreground or background to the cloud). When not considering the very low and very high values, we find a mean value for our sample of about $15 M_{\odot}/pc^3$, which corresponds to $600 cm^{-3}$.

The densities of material above the star formation threshold are naturally higher. We find a range from $23 M_{\odot}/pc^3$ (Monoceros) to $6500 M_{\odot}/pc^3$ (Taurus). The median value is about $750 M_{\odot}/pc^3$ or $3 \cdot 10^4 cm^{-3}$. Here the values for the individual clouds should be considered with great care, as we find larger values for clouds with smaller distances, indicating the non-detection of higher column density material in more distant clouds (due to limited spatial resolution) and thus an underestimate of the density.

4 DISCUSSION

4.1 Star Forming properties

To investigate possible influences of cloud structure on the star formation properties we evaluate the current and potential future amount of star formation of our sample.

i) In Paper II (e.g. bottom left panel of Fig. 4) we found that our sample of clouds can be divided into two groups when considering their column density and mass distribution in the low extinction regions (A_V above 1 mag and below the star formation threshold). We indicate which cloud belongs to which group in Table 1. Clouds in group 1 have a shallow column density and mass distribution while clouds in group 2 have a steeper distribution. Hence, group 1 members have a larger amount of material at high column densities, and thus more mass potentially available for star formation. One finds that the average fraction of mass potentially involved in star formation is about two to three times higher for clouds in group 1 (see Table 4 in Paper II).

ii) We use literature data to estimate the current number of young stars and mode of star formation for each cloud. In particular the work by Kainulainen et al. (2009) and Reipurth (2008a; 2008b) have been used. It turns out that clouds in group 1 contain typically more than 100 young stellar objects and the majority of these clouds form at least one cluster of stars. Clouds in group 2 on the other hand, typically only form a few tens of stars and no clusters.

Thus, group 1 contains clouds which intensely form stars, preferably in a clustered mode, while clouds in group 2 show weaker star formation activity mostly in a distributed mode. Taurus, without a known cluster of young stars, seems to be an exception as it belongs to group 1.

4.2 Structure functions

For our structure function analysis we selected only pixel values between the self shielding column density threshold of 1 mag A_V and the individual star formation threshold for each cloud (see Paper II), as this range represents the part of the clouds where turbulence is expected to dominate the structure. We calculated the structure functions for each cloud using the three *con-noise* maps and a spatial scale range from 0.1 pc to 1.0 pc (traceable for all clouds).

Using the data shown in Table 1 we investigated possible correlations between the parameters Δ , C against the molecular cloud densities (ρ_{av} and ρ_{SF}) as well as a range of other parameters from Table 4 of Paper II. No correlations could be found. The analysis was also performed by considering two separate groups of clouds. There are no significant differences for any of the structure function parameters between the two groups. Hence, our determined structure functions are not able to distinguish between clouds that form stars in clusters or in a distributed mode.

One might expect that the values of the co-dimension C increase with distance (i.e. the fractal dimension D is decreasing), due to the change in appearance of the cloud. More distant clouds will appear to have a more simplistic structure due to details not being resolved. However, in our analysis no such trend could be found. This can be attributed to the fact that we determine the structure functions in the scale range 0.1 pc to 1.0 pc, which is resolved for all investigated clouds.

Our mean value for all clouds of $\Delta = 0.85 \pm 0.16$ is much higher than the values of $\Delta = 0$ expected by K41. Furthermore, it is inbetween the predictions of $\Delta = 2/3$ (SL94, B02) and $\Delta = 1.0$ (S08). However, the scatter in our results means the value could be

as low as $\Delta = 0.69$ or as high as $\Delta = 1.01$. For the parameter C our average of 1.92 ± 0.37 is close to the SL94 value of $C = 2.0$, while B02 theorised a value of $C = 1.0$. In S08 C is found to be ≈ 1.1 for compressive forcing and ≈ 1.5 for solenoidal forcing, both below our average value for the co-dimension. Our average is closer to the predicted value for solenoidal forcing (in particular considering the uncertainties). Hence, we conclude that the average cloud of our sample has a structure function hinting to solenoidal forcing of the turbulent field, rather than compressive driving.

4.3 Δ -variance

Using the Δ -variance technique, we identified peaks in plots of σ_Δ^2 against Δr to quantify the scale of structure in our investigated GMCs. We were only able to find peaks in σ_Δ^2 for about half the clouds. In the remainder no peaks could be identified. This could be caused by the fact that there are no dominant scales in those clouds, or that the size of the map around each cloud was too small (due to neighbouring clouds). Note that the Δ -variance will only detect dominant scales if they are significantly smaller than the map size.

Scales identified average at about 5 pc. These generally correspond to the width of a filament or sheets in the cloud rather than the length or size of the entire cloud. In the region Lupus 3, 4, 5, 6 the peaks correspond to the length of the different filaments. When we perform the Δ -variance analysis with the star density maps, dominant scales are found as well for about half the clouds. These scales are smaller and average at about 2 pc. This indicates that the star density maps trace more compact, higher extinction regions, generally the width of dense filaments.

For the mass spectral index scaling exponent α , Federrath et al. (2010) found values of $\alpha = 0.55$ for solenoidal forcing of turbulence and $\alpha = 1.34$ for compressive driving. We find a considerable variation in the measured values for α amongst our clouds. All values are below the predicted amount for pure compressive driving. However, the mean for all clouds is $\alpha = 0.54 \pm 0.27$, hence very close to the predictions for pure solenoidal driving of turbulence.

When considering the average values of α for our two groups of clouds, significant differences can be found. While the cluster forming clouds have an average of $\alpha = 0.73 \pm 0.18$, the clouds with a more distributed star formation mode have a mean of $\alpha = 0.29 \pm 0.13$ (or, when excluding the clouds with low correlation coefficient, $\alpha = 0.32 \pm 0.14$). Based on the predictions from Federrath et al. (2010), the larger value of α for the cluster forming clouds indicates an enhanced component of compressive driving compared to the clouds with a more distributed mode of star formation. We refrain from trying to estimate a more quantitative statement about the amount of contribution from compressive driving in the cluster forming clouds, since the uncertainties and scatter in our data are clearly large.

5 CONCLUSIONS

We present the homogeneous investigation of a selection of 16 nearby Giant Molecular Clouds. Utilising near infrared extinction maps made from 2MASS data with the near infrared colour excess technique, we determine structure functions and perform a Δ -variance analysis. The same clouds as in Froebrich & Rowles (2010) were investigated. They are all reasonably nearby, away from the Galactic Plane, and to the best of our knowledge there is only one cloud along each line of sight.

Using our extinction maps we identify two groups of clouds

based on the slope of their column density and mass distributions of the turbulence dominated (low A_V) part of the cloud. We find that clouds with shallower mass distributions form stars preferably in a clustered mode, while clouds with steep mass distributions form fewer stars and show a more distributed mode of star formation.

Structure functions determined for all clouds homogeneously within a range from 0.1 pc to 1.0 pc cannot be used to distinguish clouds with different star formation modes. Comparing the structure function parameters to model calculations suggests that the turbulence in the investigated clouds is governed preferably by solenoidal forcing.

Our results of the Δ -variance analysis also indicate that the average cloud in our sample is governed by solenoidal forcing. However, clouds which form a large number of stars in clusters have an enhanced component of compressive driving of the turbulent field, in comparison to clouds with isolated star formation. Hence, compressive driving seems to lead to a more clustered mode of star formation.

To quantify these qualitative findings, i.e. to determine the fraction of solenoidal and compressive driving in each cloud, a more detailed comparison of the numerical simulations with the observational data needs to be performed. In particular viewing angle and resolution/distance effects in the model data need to be investigated.

ACKNOWLEDGEMENTS

JR acknowledges a University of Kent scholarship. This publication makes use of data products from the Two Micron All Sky Survey, which is a joint project of the University of Massachusetts and the Infrared Processing and Analysis Center/California Institute of Technology, funded by the National Aeronautics and Space Administration and the National Science Foundation.

REFERENCES

- Anselmet, F., Gagne, Y., Hopfinger, E. J., Antonia, R. A 1984, J.Fluid Mech, 140, 63
- Benzi, R., Ciliberto, S., Tripiccone, R., Baudet, C. 1993, PhRvE, 48, 29
- Boldyrev, S. 2002, ApJ, 569, 841
- Brandenburg, A. and Nordlund, A. 2009 in Reports on Progress in Physics, 74, 1
- Dubrulle, B. 1994, Phys. Rev. Lett., 73, 959
- Elmegreen, B. G. & Scalo, J. 2004, A&A, 42, 211
- Federrath, C., Roman-Duval, J., Klessen, R. S. 2010, A&A, 512A, 81F
- Froebrich, D. and Rowles, J. 2010, MNRAS, 406, 1350F
- Goodman, A. A., Pineda, J. E., Schnee, S. L. 2009, ApJ, 692, 91
- Kainulainen, J., Beuther, H., Henning, T., Plume, R. 2009, A&A, 508, 35
- Kolmogorov, A. 1941, Dokl.Akad.Nauk SSSR, 30, 301
- Lada, C. J., Lada, E. A., Clemens, D. P., Bally, J. 1994, ApJ429, 694L
- Lombardi, M., Lada, C. J., Alves, J. 2008, A&A, 489, 143
- Ossenkopf, V., Krips, M., Stutzki, J. 2008a, A&A, 485, 719
- Ossenkopf, V., Krips, M., Stutzki, J. 2008b, A&A, 485, 917
- Padoan, P., Cambr  sy, L., Langer, W. 2002, ApJ, 580, 57
- Padoan, P., Boldyrev, S., Langer, W., Nordlund,   , 2003, ApJ, 583, 308

- Reipurth, B., 2008a, Handbook of Star Forming Regions, Volume I: The Northern Sky ASP Monograph Publications, Vol. 4. Edited by Bo Reipurth
- Reipurth, B., 2008b, Handbook of Star Forming Regions, Volume II: The Southern Sky ASP Monograph Publications, Vol. 5. Edited by Bo Reipurth
- Rowles, J. & Froebrich, D. 2009, MNRAS, 395, 1640
- Scalo, J. & Elmegreen, B. G. 2004, A&A, 42, 275
- Schmidt, W., Federrath, C., Klessen, R. 2008, Phys. Rev. Lett., 101, 4505
- She, Z.-S. & Leveque, E. 1994, Phys. Rev. Lett., 72, 336
- Skrutskie, M. F., Cutri, R. M., et al., 2006, AJ, 131, 1163S
- Stutzki, J., Bensch, F., Heithausen, A., Ossenkopf, V. 1998, A&A, 336, 697

APPENDIX A: STRUCTURE FUNCTION RESULTS

A1 Individual clouds

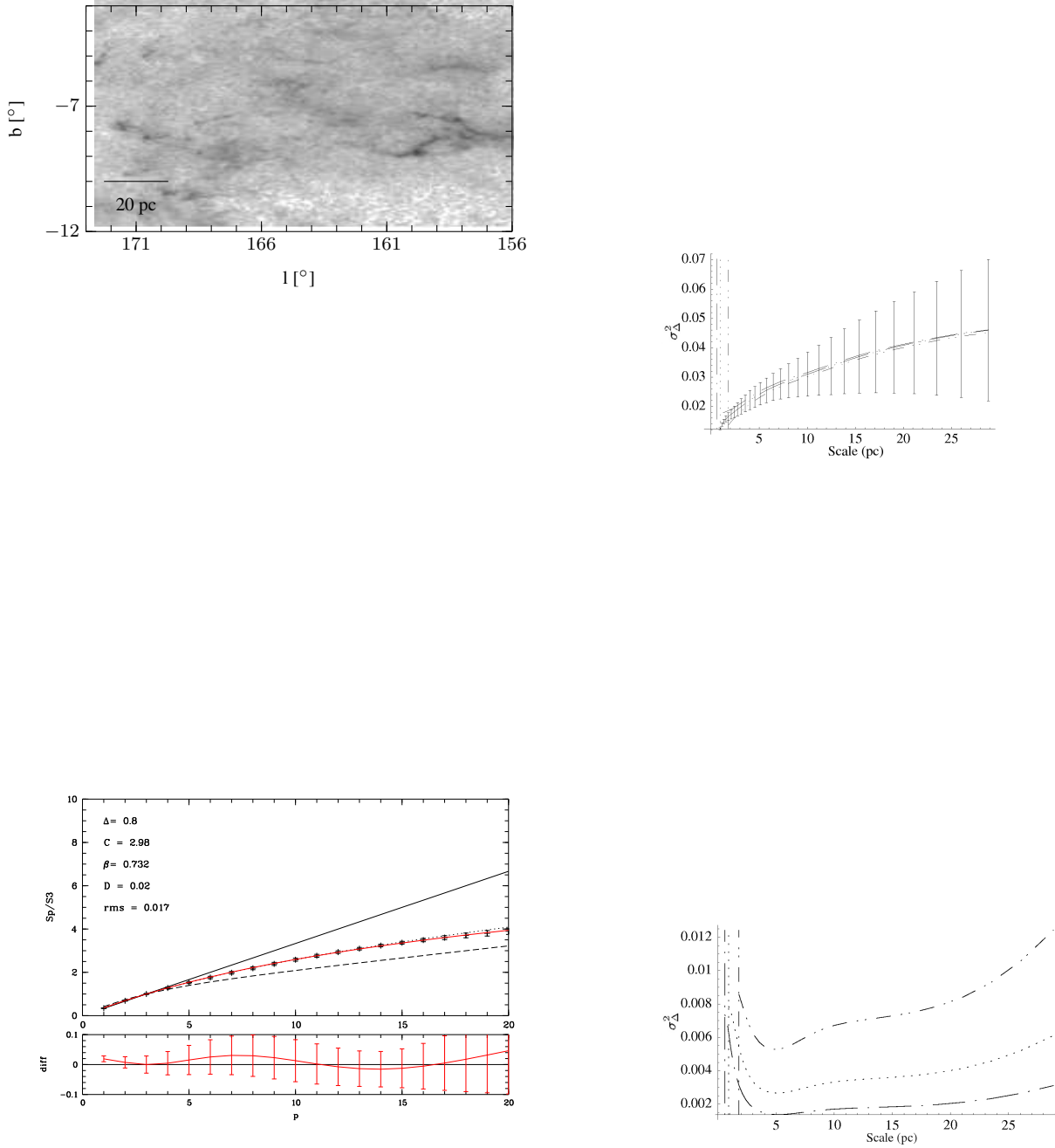


Figure A1. Sample of the Appendix. All other figures are available online only. **Top left:** An extraction of the A_V map (using the nearest 49 stars) around Auriga 1. Gray scales are square root scaled from 0 mag (white) to 15 mag optical extinction (black). The size of the image at the distance of the cloud is 133.5 pc by 70.7 pc. **Bottom left:** A plot showing the structure function $s(p)/s(3)$ against p . Our data (crosses) is compared against the models of K41 (black solid line), SL94 (black dotted line) and B02 (black dashed line). The best fit is shown as red solid line and its parameter values (Δ , C , β , D , and the rms) are listed in the upper left of the panel. The difference of the fit to the data against p is also shown as red solid line in the bottom of the panel. **Top right:** Δ -variance calculated using our *con-noise* maps. The *dash-dot* line denotes the A_V map with the nearest 25 stars used, the *dotted* line denotes the A_V map with the nearest 49 stars used, and the *dash-dot-dot* line denotes the A_V map with nearest 100 stars used. For clarity, error bars are only shown for the 49 stars data. **Bottom right:** Δ -variance calculated using our star density maps. The *dash-dot*, *dotted*, and *dash-dot-dot* lines are as in the upper right panel.